CORROSION PERFORMANCE OF PLASMA SPRAYED STELLITE COATINGS ON AZ91D MAGNESIUM ALLOY UNDER IMMERSION ENVIRONMENT

[1] K.Mathivanan *, [2] D.Thirumalaikumarasamy and [3]P.Thirumal

[1] K.Mathivanan (Corresponding Author)*
Research Scholar,
Department of Mechanical Engineering,
Government College of Engineering,
Bargur– 635104,
Krishnagiri.
Tamil Nadu,
India.
Email: mailtomathi806@gmail.com
Tel: +91-0 626089284 (Mobile)

[2]D.Thirumalaikumarasamy
Assistant Professor,
Department of Mechanical Engineering,
Government College of Engineering,
Bargur– 635104,
Krishnagiri.
Tamil Nadu,
INDIA.
Email: tkumarasamy412@gmail.com
Tel: +91-09894319865(Mobile)
Fax: +91-4144-238080/238275

[3]P.Thirumal
Associate Professor,
Department of Mechanical Engineering,
Government College of Engineering,
Bargur– 635104,
Krishnagiri.
Tamil Nadu,
INDIA.
Email: ptml76@gmail.com
Tel: +91-09443455580(Mobile)

Abstract

Stellite alloys are of great interest in industries owing to a unique combination of high temperature mechanical strength, outstanding wear and corrosion resistance. Different thermal spraying processes are used for deposition of stellite alloys on industrial components. However, the investigations on the corrosion behavior of these alloys produced via different deposition process are limited. This study focuses on the microstructure and corrosion properties of stellite powder deposited by atmospheric plasma spraying process on a AZ91D magnesium alloy substrate. The coatings were characterized by SEM, optical microscopy and atomic force microscopy. Immersion tests are performed at different pH value, chloride ion concentration and exposure time in sodium chloride environment. Moreover, XRD tests were run on the powder and the coatings to reveal possible phase transformation during spraying, as well as during corrosion test. The corrosion experiments were performed based on central composite design and response surface method to develop multiple regression models. The accuracy of the regression models was adequate through analysis of variance to make correlations between input parameters and responses. It was found that pH value greatly influences the corrosion behavior of stellite coatings followed by other parameters such as chloride ion concentration and exposure time also plasma sprayed coatings have performed better performance in corrosion tests.

Keywords: Corrosion, Plasma spraying, Stellite coating, Mg alloy

Abbreviations:

APS: Atmospheric plasma spraying process

M: Chloride ion concentration, mol

CR: Corrosion rate, mm/year

P: pH value

RSM: Response surface methodology

T: Exposure time, h

SEM: Scanning electron microscopy

1.0 Introduction

Magnesium (Mg) alloys offer the advantages of high specific strength/stiffness, better shock absorption, and easy processing, attracting increasing interest for use in the automotive, aerospace, electronics, and transportation industries. However, their wider industrial applications are severely limited by their poor corrosion and wear resistance performance. Surface coating is an effective method to improve the comprehensive performance of Mg alloys. The common surface treatment methods used on Mg alloys mainly include vapor deposition, anodic oxidation, micro arc oxidation, electro deposition, chemical conversion coatings, and thermal spraying. Among the above mentioned various surface techniques, atmospheric plasma spraying is considered as an effective method to prevent corrosion of magnesium and its alloys [1].

Distinctive alloys are frequently used for coating machine elements to improve their life expectancy in service. Stellite is a CoCrWC alloy with outstanding corrosion, wear, and oxidation resistance over a wide temperature range, especially for high demand requests. Chromium provides mechanical strength and corrosion resistance; tungsten increases the strength of Co–Cr by solid solution strengthening. Besides its use in bulk form, Stellite coatings have become an essential factor for the manufacturing and repair of equipment, leading to the enhanced performance of equipment components like turbine blades and vanes, as reported by Shidu et al. (2006) and Mirshekari et al. (2017) [2, 3]. Different technologies can successfully deposit Stellite coatings onto a component surface and imply a large variation in the properties of the deposited material. Furthermore, some technologies present higher productivity regarding material deposition rate, like plasma spraying process that is the state of art for several industrial demands.

Stellite alloys are deposited by different liquid state deposition techniques like welding [4-6], thermal spraying [7-9], supersonic laser deposition [10], and solid-state processes including friction surfacing [11] and explosive welding [12]. Different process leads to different tribo mechanical and structure property [13, 14]. The chemical composition of the coating is changed due to the substrate dilution during the welding of Stellite alloys. So, the phase transformation capability and galling resistance of the deposited layer are less than those of the original alloy [15]. Moreover, multi-layer deposition or low heat input techniques (e.g. cold metal transfer welding process) are suggested for diminishing the dilution of the coating [16, 17]. The multi-layer technique increases the cost and the time of deposition. In cold metal transfer welding process, tensile residual stress is developed in the coatings, and underbead cracks are observed on the stellite alloy deposited on heat treated steel substrates [18]. It means that hardfacing of heat treated steel by liquid state process is impossible even with low heat input [19, 20]. The limitation of explosive welding from the viewpoint of safety regulations [21, 22] and also friction surfacing applicability only for simple flat geometries [23, 24] compel the researchers to use new methods. Therefore, thermal spray methods are suggested and used by different authors [25-29].

Various corrosion tests have been performed to study the corrosion performance of the thermally sprayed coatings on magnesium alloys. D'Oliveira et al. (2002) [30] used plasma transferred arc (PTA) for the application of stellite coatings aiming the study of their high-temperature behavior. Bartkowski and Bartkowska (2017) [31] studied the wear resistance of laser cladded stellite coatings. Also, Gas Tungsten Arc Welding (GTAW) cladding and thermal spray technology have been extensively used. Especially for wear resistance applications, Stellite has been receiving even more attention based on the possibilities that open up by varying application processes or composition with other

materials. Zhao et al. (2013) [32] proved the benefits of a thermally sprayed Stellite coating on a desulfurization slurry circulating pump that improved the erosion, cavitation and corrosion performance of the pump. Ciubotariu et al. (2016) [33] applied the same coatings by HVOF on hydropower plant components for cavitation protection and reported a promisor result mainly for additional laser remelting of the coating surface. The authors showed that corrosion resistance, although better than the martensitic substrate, should be taken care of pitting in the coating layer.

According to the literature review, [4–33] it is understood that most of the published works have focused on the corrosion behavior of thermal sprayed coatings on magnesium alloys. From a practical view point, it is worthwhile to investigate and understand the effect of environmental factors on the corrosion behaviour of surface treated magnesium alloys. To date, however, there is not much published information on the effect of pH, chloride ion concentration and exposure time on the corrosion of surface treated magnesium alloys. Hence, the present investigation was carried out to develop an empirical relationship to predict the corrosion rate of plasma sprayed stellite coatings on AZ91D magnesium alloy under immersion environment. The effect of pH value, chloride ion concentration and exposure time on the corrosion behaviour of plasma sprayed stellite coatings is detailed in this article.

2.0 Experimental procedures

The chemical compositions of the AZ91D alloy used in this study are as follows: Mg-8.3Al–0.35Zn–0.15Mn (wt-%). The cut sectional surface of AZ91D magnesium alloy sheets (16×15×4 mm) was grit blasted using cabinet type grit blasting machine before plasma spraying. Grit blasting was carried out using corundum grits with size of 500±320 mm and subsequently cleaned using acetone in an ultrasonic bath and dried. In the APS method, the maximum operating pressure (40bar) and temperature (800°C) of

the process gas were used. One-layer

spraying performed at 10mm stand-off distance and 100mm.s^{-1} nozzle traverse speed. The nozzle was moved 1.5mm in each pass to achieve a uniform coating. These parameters were selected according to our previous work to achieve a coating with the best adhesion and lowest porosity [34]. The optical micrograph of the coating produced under optimised plasma spray parameters is shown in Fig. 1a. Photographs of plasma treated specimens are displayed in Fig. 1b and c. In this investigation, stellite powders with size range of -45±20 mm have been deposited on grit blasted magnesium alloy substrates. Plasma spraying has been performed using an APS system 40 kW insulated gate bipolar transistor based Plasmatron (Ion Arc Technologies, India; model: APSS-II) as shown in Fig. 2.

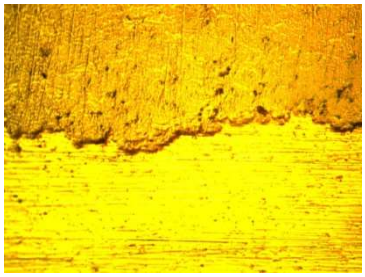

(a) Optical micrograph of the coating produced under optimised plasma spray parameters

(b) Uncoated specimens

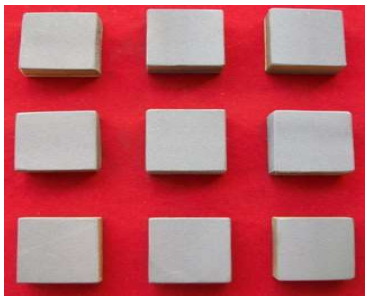

(c) Coated specimens

Fig.1 Experimental

(a) Plasmatron spray unit used to deposit coatings

Fig.2 Thermal spray facility used in this research

Coating thickness for all the deposits was maintained at 200±15 mm. This was achieved using the following method. The values of the factors were set in the machine as prescribed by a run in the design matrix, after which one single layer was made. The gun traverse rate was constant for all experiments; it was 300 mm s^{-1}, and the coating track overlap was 30%. The thickness of the single layer made after the run was measured using a digital micrometer (model DIGIMATIC MDC-25SB). The number of passes required to achieve 200 mm thickness was determined, and the spray run was carried out to achieve it.

In this study, a spherical morphology powder (Metalizing Equipment Company Pvt Ltd, India) with the chemical composition of Stellite 21 was used. The chemical composition of the feedstock (in wt.%) was 28 Cr, 5.5 Mo, 2.5 Ni, 0.3C, 1 Si, Fe<2, W<0.5, and balance Cobalt. AZ91D magnesium alloy substrate plate of 20×50×4 mm^3 was used as substrate. The substrate was sandblasted by alumina. The as sprayed samples were cut and mounted in the resin. The mounted samples were prepared in accordance with the ASTM E3-95 [35] and subsequently grinded on emery paper (120, 240, 600, 1200 grit) and polished by 6 and 1μm monocrystalline diamond suspensions, respectively. The polished cross sections were investigated by optical and scanning electron microscopes

to find the effect of spraying method on the coatings microstructure, the amount of porosity and coating integrity. The thickness of the coatings was measured on 200× magnified OM micrographs using image analysis software. The images were obtained along the coating cross section and the average of five measurements was reported. Also the average value of the coatings porosity on 1000× magnification at 20 different areas was reported (Fig.3).

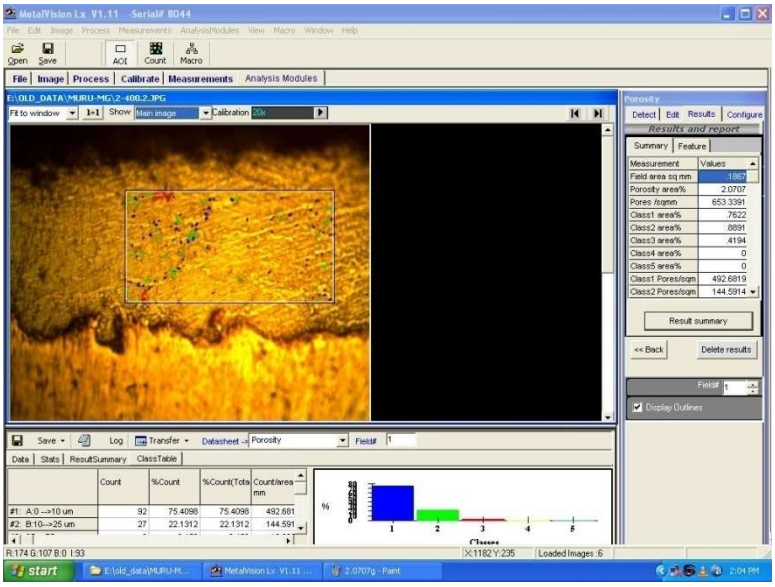

Fig.3 Porosity analysis

Vickers micro hardness profile measurement was carried out on the cross section of the coating. This measurement was repeated in three lines and the average value of them is reported. The distance of 100μm was selected between the indentations to avoid a mutual influence of indented points to the results. The load of 100grf was applied for 15s.

Immersion corrosion test was carried out as per the ASTM standard G31-72 [36] to evaluate the corrosion behaviour of the stellite coated Mg alloys. The corrosion stability of coated samples was investigated using a immersion test in NaCl solution at different chloride ion concentrations, pH value and exposure time. For each experimental condition, two coated specimens were prepared and tested.

The specimens were cut into the dimensions of 16 x 15 x 4 mm to evaluate the corrosion rate by immersion corrosion test methods. The corrosion test specimens for immersion

corrosion tests are shown in Fig. 4. The specimens were ground with 500#, 800# and 1200#, 1500# grit SiC paper washed with distilled water and dried by warm flowing air before the corrosion experiment was carried out.

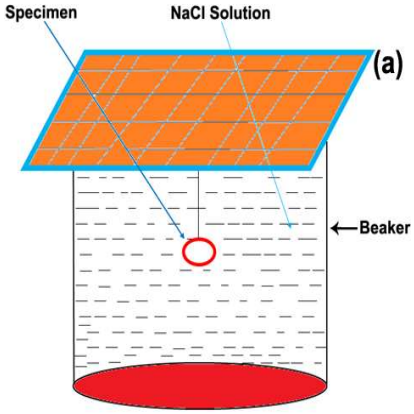

Schematic diagram of test set up

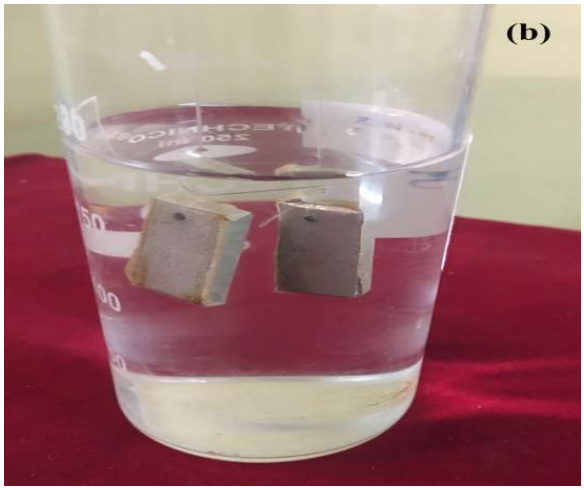

Photograph of test set up

Specimens of uncoated and coated speimens after immersion corrosion test

Fig. 4 Test set up and specimen during the immersion corrosion test

2.1 Finding the limits of corrosion test parameters

Based on the literature review [4-33], and the previous investigation carried out in our laboratory [37] the predominant factors that have a greater influence on the corrosion behavior were identified. They are: (i) pH value of the solution, (ii) chloride ion concentration and (iii) exposure time. Large number of trial experiments were conducted to identify the feasible testing conditions for AZ91D magnesium alloy under immersion

test conditions. The following inferences were obtained:

1. If the pH value of the solution was less than 3, the change in chloride ion concentration did not considerably affect the corrosion.
2. If the pH value was in between 3 and 11, there was inhibition of the corrosion process and stabilization of the protective layer
3. If the pH value was greater than 11, then blocking of further corrosion by the active centres of protective layer.
4. If the chloride ion concentration was less than 0.2 M, then the visible corrosion did not occur in the experimental period.
5. If the chloride ion concentration was in between 0.2 M and 1 M, then there was a reasonable fluctuation in the corrosion rate.
6. If the chloride ion concentration was greater than 1 M, then the rise in corrosion rate may hesitate and decrease a little.
7. If the exposure time was less than 2 hours, then the surface was completely covered with thick and rough corrosion products.
8. If the exposure time was in between 48 and 168 hour, then the tracks of the corrosion can be predicted.
9. If the exposure time was greater than 168 hours, then the tracks of corrosion film were difficult to identify

2.2 Developing the experimental design matrix

As the range of individual factor was wide, a central composite rotatable three-factor, five-level factorial design matrix was selected. The experimental design matrix consisting 20 sets of coded condition and comprising a full replication three- factor factorial design of 8 points, 6 star points, and 6 center points was used. Table 1 represents the range of factors considered, Table 2 show the 20 sets of coded and actual values used to conduct the experiments. The upper and lower limits of the parameters were coded as +2 and –2, respectively. Thus, the 20 experimental runs allowed for the

estimation of the linear, quadratic, and two-way interactive effects of the variables. Tables 3 and 4 presents the ANOVA test results for corrosion rate of uncoated and coated AZ91D magnesium alloy. Developed mathematical equations to predict the corrosion rate is given below,

Table 1 Immersion corrosion test experimental parameters and their levels

S. No.	Factor	Unit	Levels				
			−2	−1	0	1	2
1	pH value	pH	3	5	7	9	11
2	Exposure time	hours (h)	48	72	120	144	168
3	Cl^- concentration	Mole (M)	0.2	0.4	0.6	0.8	1

Table. 2 Design matrix and test results for immersion corrosion

Experiment condition	Original values			Corrosion rate for Uncoated AZ91D Magnesium alloy (mm/year)	Corrosion rate for coated AZ91D Magnesium alloy (mm/year)
	(pH)	(M)	(hour)		
1	5	0.4	48	7.94	2.18
2	9	0.4	48	5.24	1.44
3	5	0.8	48	15.40	4.23
4	9	0.8	48	10.31	2.83
5	5	0.4	144	6.20	2.79
6	9	0.4	48	3.23	1.45
7	5	0.8	48	11.86	3.26
8	9	0.8	47	7.22	3.97
9	3	0.60	72	15.85	8.71
10	11	0.60	72	4.14	2.07
11	7	0.20	72	4.74	2.60
12	7	1.00	72	14.61	6.57
13	7	0.60	48	10.92	4.91
14	7	0.60	168	5.02	2.51
15	7	0.60	120	3.11	1.71
16	7	0.60	120	5.43	2.71
17	7	0.60	120	5.47	3.01
18	7	0.60	120	5.33	2.66
19	7	0.60	120	5.16	2.33
20	7	0.60	120	5.13	2.3

Responses = f (P, M and T)

Corrosion rate (AZ91D magnesium alloy) = $0.21-0.076* P + 4.956x10^{-3}* M - 4.381 \times10^{-3}* T + 8.611 \times10^{-3}* P^2 + 5.549 \times10^{-3}* M^2 - 3.252 \times10^{-4}*T^2 - 0.016* P * M + 7.087 \times10^{-3}* P * T + 0.022* M * T$……(1)

Corrosion rate (Stellite coatings) = $0.19 + 0.016* P + 0.025 * M - 0.033* T + 0.031* P^2+ 1.857 \times10^{-3}* M^2 + 4.253 \times10^{-3} * T^2 - 0.013* P * M + 0.035* P * T + 4.000 \times10^{-3} * M * T$…….(2)

Table 3 ANOVA results for uncoated AZ91D Magnesium alloy

Source	Sum of squares	df	Mean Square	F-value	Prob > F	
Model	300.3993	9	33.3777	23.24706	< 0.0001	Significant
A	90.17218	1	90.17218	62.80356	< 0.0001	
B	109.8828	1	109.8828	76.53171	< 0.0001	
C	30.15766	1	30.15766	21.00436	0.0010	
A^2	39.41379	1	39.41379	27.45111	< 0.0004	
B^2	32.80786	1	32.80786	22.85018	0.0007	
C^2	12.84216	1	12.84216	8.944368	0.0136	
AB	2.06045	1	2.06045	1.435072	0.2586	
AC	0.00405	1	0.00405	0.002821	0.9587	
BC	1.0368	1	1.0368	0.722115	0.4153	
Residual	14.35781	10	1.435781			
Lack of Fit	10.25133	5	2.050266	2.496377	0.1691	not significant
Pure Error	4.106483	5	0.821297			
Cor Total	314.7571	19				

Table 4 ANOVA results for coated AZ91D Magnesium alloy

Source	Sum of squares	df	Mean Square	F-value	Prob > F	
Model	82.73188	9	9.192431	487554.3	< 0.0001	Significant
A	25.85723	1	25.85723	1371433	< 0.0001	
B	29.00361	1	29.00361	1538313	< 0.0001	
C	7.554252	1	7.554252	400667.5	< 0.0001	
A^2	14.455	1	14.455	766674.1	< 0.0001	
B^2	7.814036	1	7.814036	414446.1	< 0.0001	
C^2	2.86998	1	2.86998	152219.9	< 0.0004	
AB	0.763848	1	0.763848	40513.48	0.0011	
AC	0.025765	1	0.025765	1366.515	< 0.0001	
BC	0.656658	1	0.656658	34828.27	< 0.0001	
Residual	0.000189	10	1.89×10^{-5}			
Lack of Fit	3.08x10-6	5	6.16 x10-7	0.0166	0.9998	not significant
Pure Error	0.000185	5	3.71 x10-5			
Cor Total	82.73206	19				

3.0 Results and Discussion

3.1 Microstructure

Fig. 5 illustrates the SEM image of the prealloyed Stellite 6 superalloy powder used in the experiments. It was seen in the SEM images that Stellite 6 powders had a spherical form. The EDX analyses proved higher content of Ni and W (20 wt.% and 5wt.%), indicating the impurities in the feedstock powder.

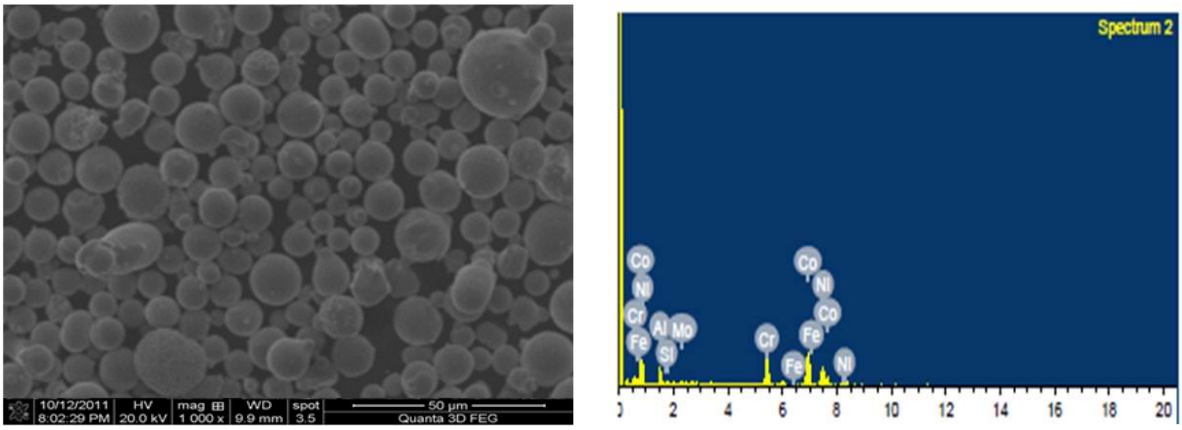

Fig. 5 SEM micrograph of Stellite powder

Most probably, the foreign particles intrude into the Stellite 6 powder in the powder feeder, as a residue after previous spraying experiments with powder of different

composition. The microstructure of as-sprayed coating can be seen in Figure 6.

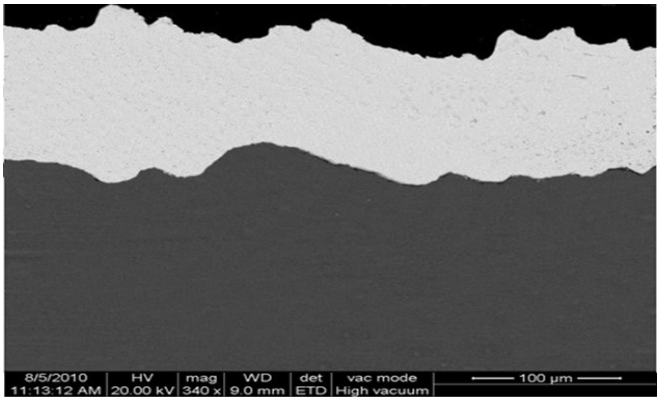

Fig. 6 Cross section as-sprayed Stellite coating

The coating consists of individual splats. On the intersplat boundaries, a minor porosity is concentrated. On the boundary between the coating and substrate, the α-Al_2O_3 particles were occasionally observed, embedded into the substrate material during the grit blasting procedure. Analysis of microstructure and energy-dispersive x-ray spectroscopy (EDX) patterns revealed that the produced stellite coating had a lamellar structure consisting of α-Co and ε-Co phases and chromium-rich carbides (Fig.7). The phase composition of as-sprayed coating consist of the two kinds of Co-based solid solution, original face centered cubic (fcc) and during spraying developed hexagonal close packed (hcp) phase, in the mutual ratio 70/30, while the original powder was composed of only fcc based solid solution.

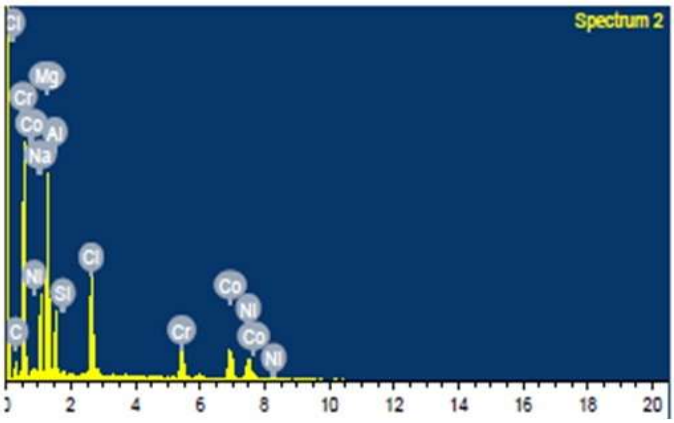

Fig. 7 EDS analysis of coating

In the literature, the existence of two allotropic modification (high temperature fcc phase and the low-temperature hcp phase) of pure Co and its alloys is described. At room temperature in polycrystalline Co, the metastable fcc phase is often present, stabilized when the grain size is reduced and its stability is further fostered by the addition of C, Ni and Fe in Co-based alloys. On the other hand, addition of Cr, Mo and W into the alloy tends to stabilize the hcp structure. The plasma sprayed Stellite 6 coatings microstructure is reported to consist of fcc Co-rich phase, pure or containing small amount of carbides. In the as sprayed coatings microstructure, the white splats was observed, randomly distributed in the coatings cross section.

3.2 Immersion Corrosion Test

3.2.1 Effect of pH Value on Corrosion rate of Immersion Corrosion

In order to study the effect of pH, chloride ion concentration and exposure time was kept constant at 0.6 M, 120 hrs while the pH level was varied from 3-11. Figure 8 compares the effect pH value on the corrosion rate.

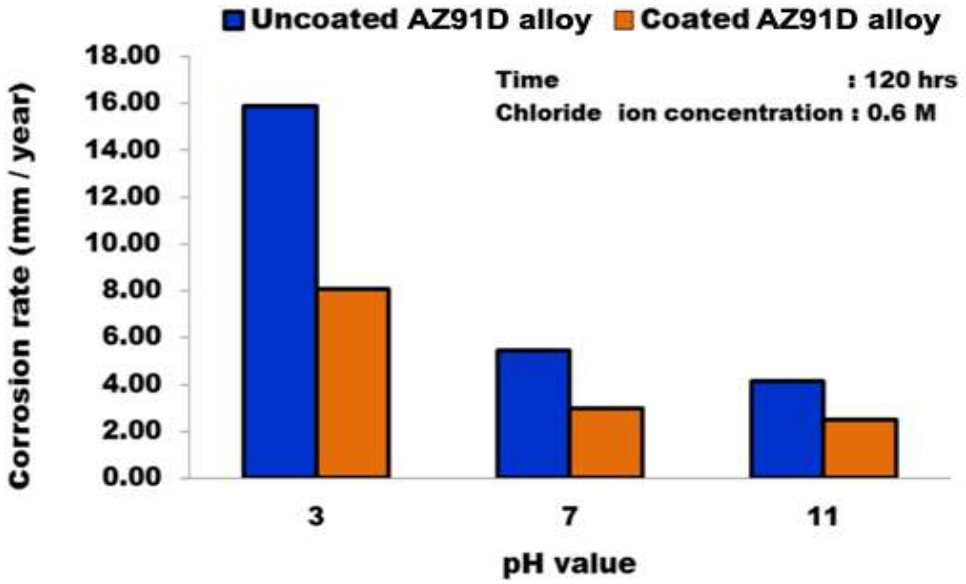

Fig. 8 Effect of pH value on corrosion rate

From the experimental results and fundamentals, it is acknowledged that the low pH value can promotes corrosion and high pH value exhibits moderate corrosion loss in both coated and uncoated AZ91D magnesium alloy. Figure 9 shows the SEM images of the corroded uncoated and coated AZ91D magnesium alloy immersed in NaCl solution. At low pH value, a brown tarnish color change was noted on the surface of the uncoated AZ91D magnesium alloy. This color change is owing to the progression of the uniform dezincification and the sharp line of separation between the dark dezincified materials. This dezincification was occurred due to the presence of $MgCl_2$ in the solution and this might be interpreted as an evidence of Mg+ exchange or dissolution into the electrolyte. These chloride layers are responsible to destroy the Mg passive film (Fig.9 (a)), especially in the acidic solutions that leads to higher rate of corrosion. At lower pH value of stellite coated AZ91D magnesium alloy, corroded samples shows the corrosion spots. Slight discoloration was observed in the WC coating surface after the test at initial stages. In stellite coatings, corrosion proceeds primarily by dissolution of the Cr phase and removal of W particles in the matrix. The removal of W particles in Fe-Cr binder matrix is shown Fig. 9(b). At lower pH values, the presence of oxidizers enhances the oxidation reactions in the acidic solutions, leading to high corrosion rate. At neutral pH, in the initial stage a noticeable discoloration was observed at the top of the surface of bare AZ91D magnesium alloy substrate. The protective surface layers present in the top of the AZ91D magnesium alloy. These corrosion products could react with aggressive chloride ions from contaminated soluble NaCl to form insoluble Magnesium chloride hydroxide providing protectiveness to the substrate and reduces aggressive soluble chlorides. Hence, moderate corrosion was observed in the uncoated AZ91D magnesium alloy [38-40].

At neutral pH level, true passivity is not exhibited by the coating suggests that the corrosion film is not continuous over the entire matrix. Fe-Cr binder matrix loses its Cr when it is exposed to chloride environment and forms Cr_2O_3. It has reported that the formation of Cr_2O_3 in stellite based coatings takes place as small islands are spread non-uniformly over the surface. Formation of chromia nullifies the corrosion rate. At higher pH level, a thick gold colored layer formed over the surface of both uncoated and coated layer is the evidence of formation of corrosion product as shown in the Fig. 9 (c). Iron and chromium whenever exposed to chloride ion environment tends to form its chloride layers. Eventually, oxides of chromium and iron was destroyed and corrosion was observed. Stellite coated AZ91D magnesium alloy exposed to the chloride containing environment, formation of chloride layer over the binding metals are unable to destroy the excellent corrosion resistance metal oxides. Thereby, corrosion rate in coated AZ91D magnesium alloy shows low. However, some pits, pores and splat ejection was observed in Fig. 9 (d) through these electrolyte can permeate into the coating and forms galvanic coupling between metals and corrosion is recorded. Atomic microscopy analysis was carried out on the top surface of the corroded specimens to understand the nature of material removal from the surface.

Un coated AZ91D Magnesium alloy

pH value= 3 Corrosion time= 120 (h) Cl^- concentration = 0.6 (M)

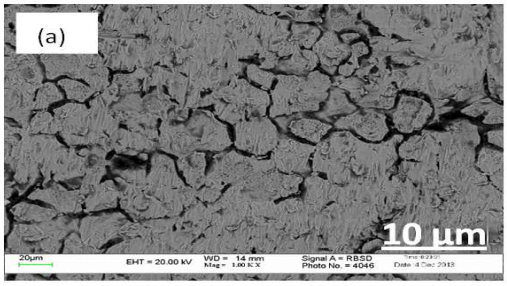

Coated AZ91D Magnesium alloy

pH value= 3 Corrosion time= 120 (h) Cl^- concentration = 0.6 (M)

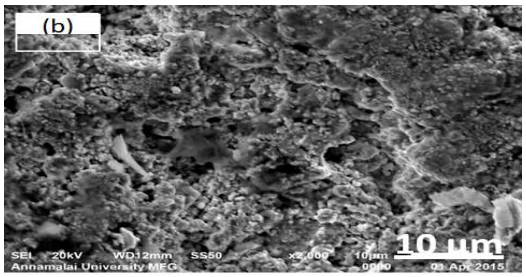

Un coated AZ91D Magnesium alloy

pH value= 11 Corrosion time= 120 (h) Cl^- concentration = 0.6 (M)

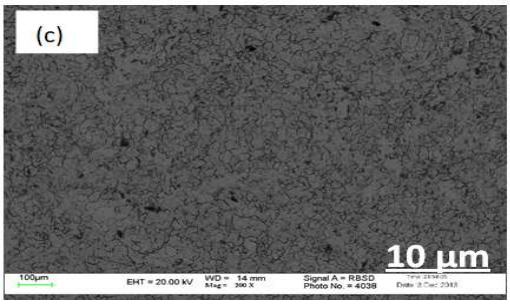

Coated AZ91D Magnesium alloy

pH value= 11 Corrosion time= 120 (h) Cl^- concentration = 0.6 (M)

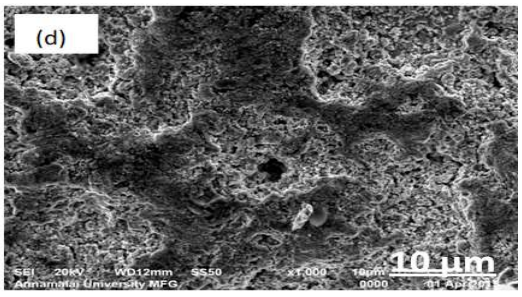

Fig. 9 Effect of pH on corroded surface in immersion corrosion tests

Figure 10(a) reveals the effect of pH value on corroded surface of uncoated AZ91D magnesium alloy. From the image it is inferred that AZ91D magnesium alloy experiences higher material removal and can be visualized in the form the higher 'Ra' whereas Fig. 10 (b) corresponding to coated AZ91D magnesium alloy shows lower surface roughness value when compared with bare substrate and its material loss. Though the pit depth is shallow in the coated surface, the region in the coating exposed to corrosion medium is also affected. At higher pH level, low corrosion rate was observed, but undulation level is minimum.(Fig.10 c and d).

From the fundamentals, the pH value has an inverse proportional relationship with the corrosion rate; i.e., if the pH value is increases, the corrosion rate is decreases.The highest corrosion rate was observed at pH 3 and at neutral pH, the corrosion rate was remained constant approximately and comparatively low corrosion rate was observed in alkaline solution. It is suggested that the influence of pH in corrosion rate is high at higher concentration when compared with low concentration in neutral and alkaline solutions. In accordance with this, the AZ91D magnesium alloy corrosion domains of selective leaching of chromium and dissolution of both iron and chromium can be observed.

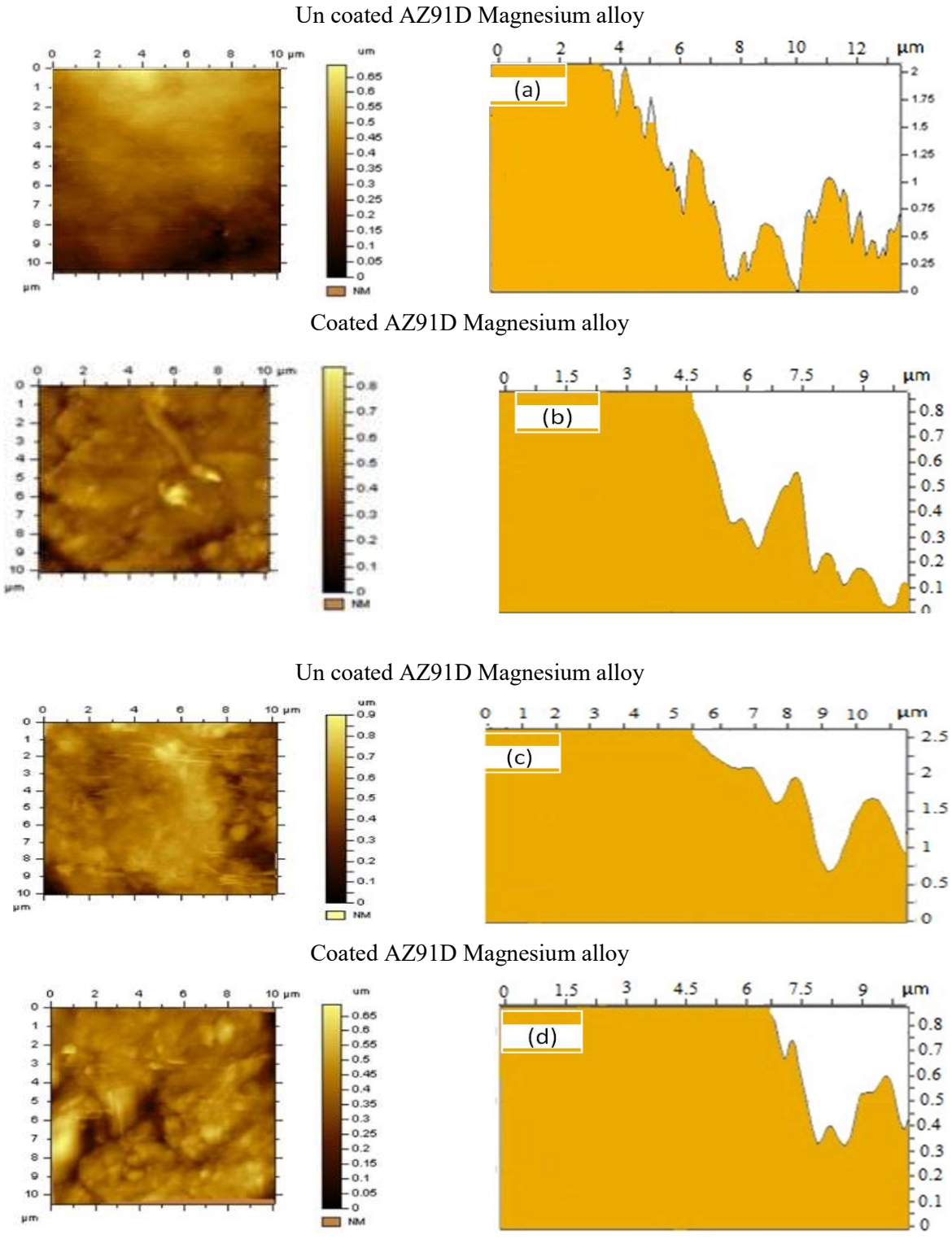

Fig. 10 AFM images of corroded specimens exposed to various pH levels

Figure 11 shows the regions where the corrosion products are actively formed at various pH levels. Figure 12 shows the regions where the metal will freely corrode; the region of passivation where stable oxide or other films form and the corrosion process is stifled; the region of pitting corrosion where the corrosion potential of the metal exceeds that of its oxide; and the region of immunity where the metal is normally fully safe to use (Fontana, 1986) **[41]**.

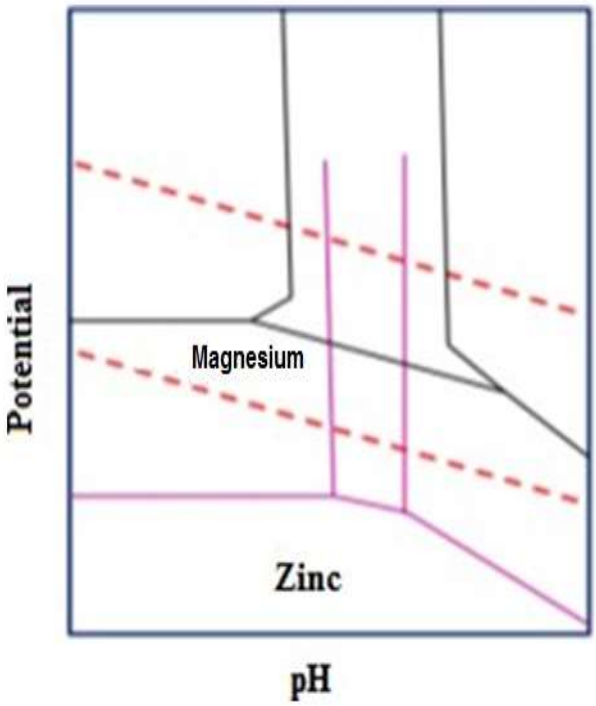

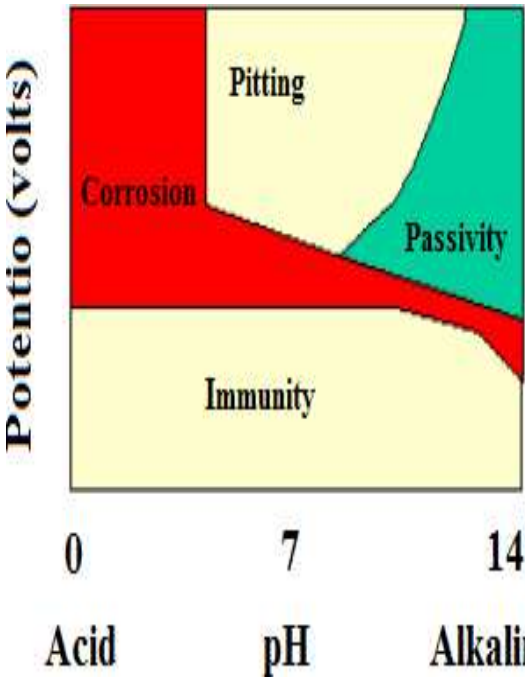

Fig. 11 Effect pH on corrosion potential

Fig. 12 Potential Vs pH

3.2.2 Effect of Chloride ion concentration on Corrosion rate of Immersion Corrosion

The influence of chloride ion concentration on corrosion rate of uncoated and coated AZ91D magnesium alloy alloy is displayed in Fig. 13.

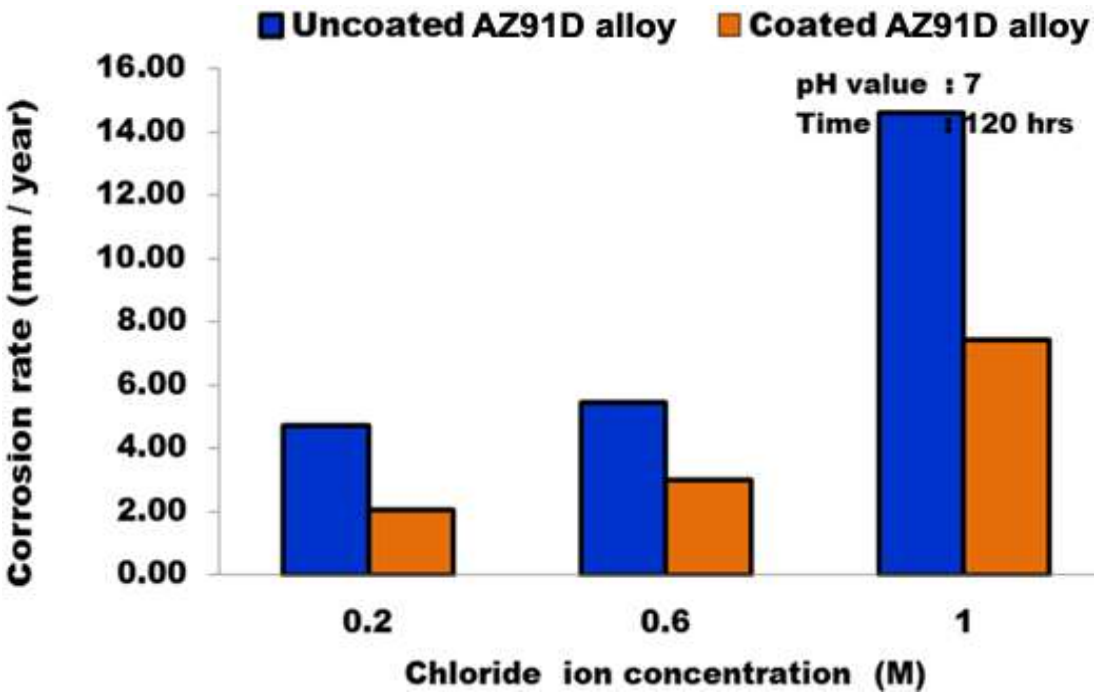

Fig. 13 Effect of chloride ion concentration on corrosion rate

To investigate the effect of chloride ion concentration, the pH value and exposure time was kept constant at 7, 120 hr while the chloride ion concentration was varied from 0.2 to 1 M. Fig. 9 compares the effect of chloride ion concentration on the corrosion behavior. Increasing chloride ion concentration in the corrosion environment, uncoated AZ91D magnesium alloy and coated naval bras corrosion rate is increased. Introduction of stellite coatings over the exposed area of the AZ91D magnesium alloy could protect the metal around 42% from its degradation. At low chloride ion concentration level, the corrosion rate is low when compared to the high level. The top surface of the AZ91D magnesium alloy is exposed to NaCl solution shows remarkably less attack than the remaining region, but the general corrosion attack was noticeable. Some macro pits can be seen in Fig. 14 (a). Chloride ion containing environment is very aggressive to the AZ91D magnesium alloy alloy, less chloride ions means less attack over the exposed region. Hence, the corrosion rate is minimum at low chloride ion concentration tests. Hence, decrease in chloride ion concentration, the ions becomes less aggressive and lose

their tendency to dissolute the corrosion resistant layer as evidenced by the corroded surface examination. In coated AZ91D magnesium alloy, the mechanism of attack was associated with severe corrosion of the matrix which is shown in black colour is leaving the white hard phase particles. Figure 14 (b) demonstrates the initiation of matrix corrosion (shown by light brown colour) within a splat. It seems to be clear that the corrosion could takes place around the splat boundary in the dense hard phase matrix which will lead to a macro pit. From the morphological studies, it was observed that at higher concentration, the surface of the specimen severely corrodes. At lower chloride ion concentration, the pit seems to be narrowed. But in higher concentration the pit became widen and shallow. Also, the pit depth increases with the increase in the concentration of the solution as shown in Fig.14 (c). Figure. 14 (d) shows pitting in micro scale after the hard particles being dislodged from the surrounding matrix due to micro-galvanic attack at the hard particle / matrix interface. Figures 15 (a-c) shows the AFM images of the corroded specimens top surface. It is evident from the "Ra" values, AZ91D magnesium alloy experiences material loss at low and higher level of chloride ion concentration. The adsorption of chloride ions in to oxide, covered Mg, surface transformed Mg $(OH)_2$ to easily soluble $MgCl_2$, thus destroying the compactness of the corrosion product film and resulting in pitting corrosion. The pit depths were in the range of 3-6 μm, which suggests the removal of individual splats. On the exposed area, macro-pit formation in the form of splat boundary attack and the eventual fall (flaking) of the whole can be seen as dark areas. The increasing trend of the pit depth with the increase in chloride ion concentration is attributed to the attack of Cl^- ions on the surface leading to the anodic dissolutions of magnesium alloy. [42, 43]

Un coated AZ91D Magnesium alloy
pH value= 7 Corrosion time= 48(h) Cl^- concentration = 0.2(M)

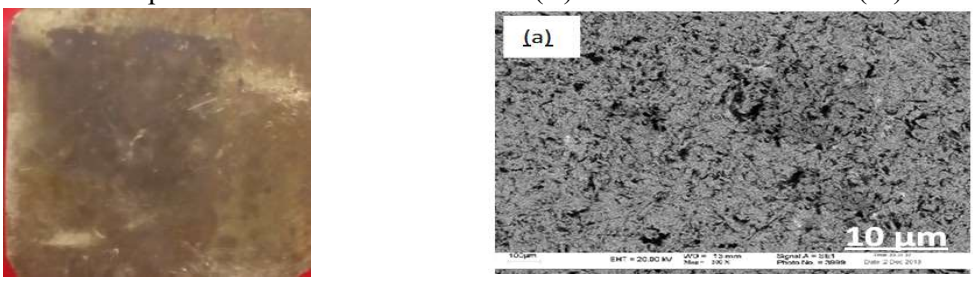

Coated AZ91D Magnesium alloy
pH value= 7 Corrosion time= 48(h) Cl^- concentration = 0.2(M)

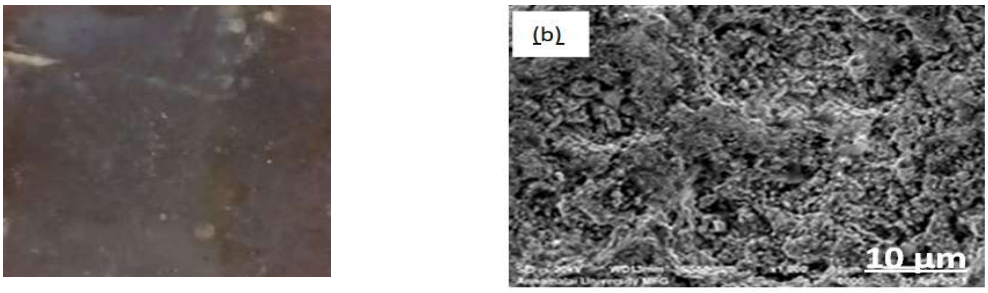

Un coated AZ91D Magnesium alloy
pH value= 7 Corrosion time= 48(h) Cl^- concentration = 1(M)

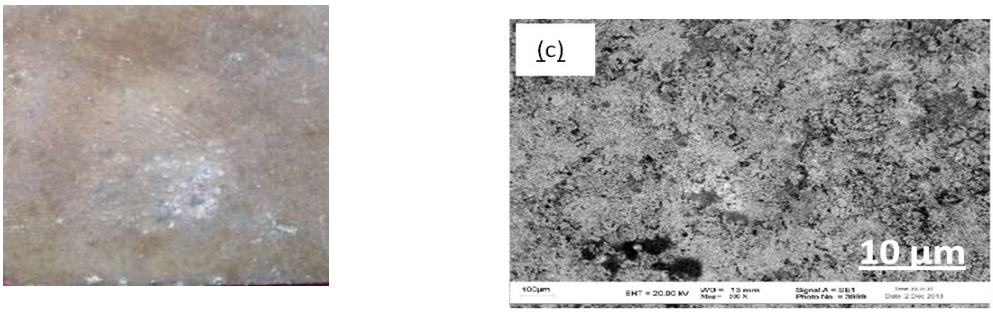

Coated AZ91D Magnesium alloy
pH value= 7 Corrosion time= 48(h) Cl^- concentration = 1(M)

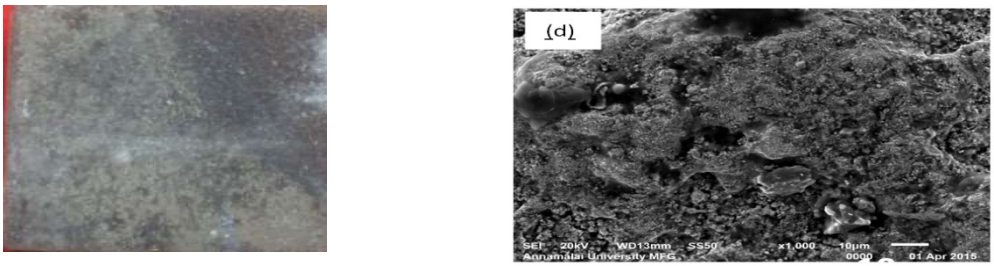

Fig. 14 Effect of chloride ion concentration on corrosion morphology of uncoated and coated AZ91D magnesium alloy

Un coated AZ91D Magnesium alloy

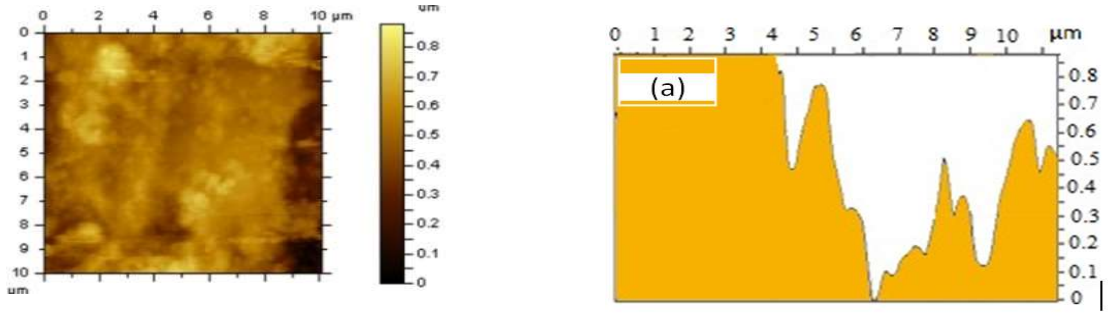

Coated AZ91D Magnesium alloy

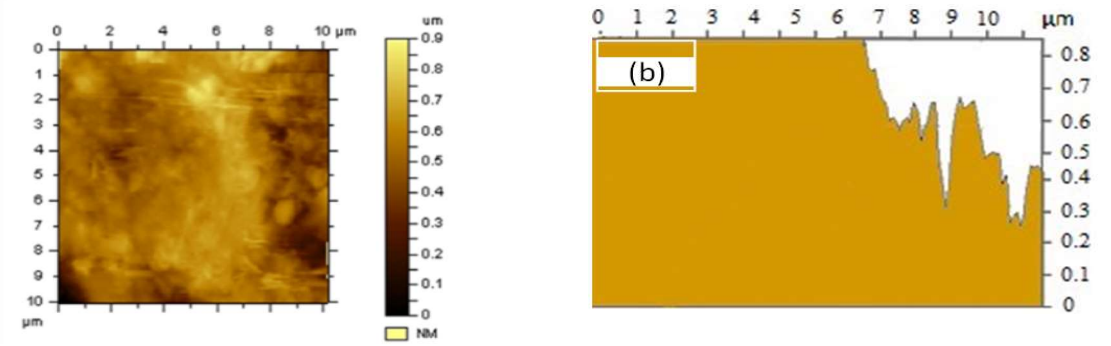

Un coated AZ91D Magnesium alloy

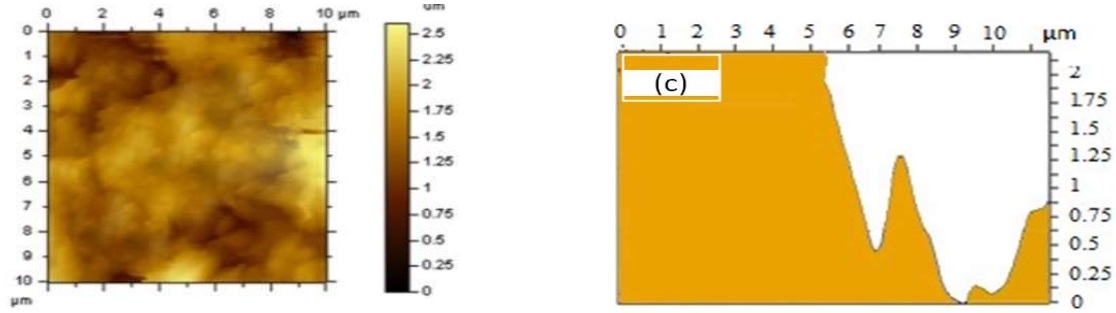

Coated AZ91D Magnesium alloy

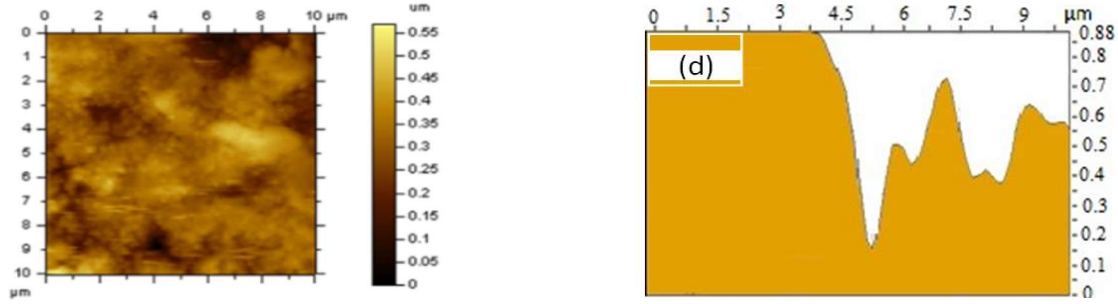

Fig. 15 AFM images of corroded specimens exposed various Cl^- ion concentration

3.2.3 Effect of exposure time on Corrosion rate of Immersion Corrosion

The effect of exposure time on corrosion rate is displayed in Fig. 16. It is observed that increasing exposure time is ultimately increases the material loss to the uncoated and coated AZ91D magnesium alloy. In order to examine the effect of time, pH value and chloride ion concentration was kept constant at 7, 0.6 M. The exposure time was varied from 24 to 72 h. Depositing productive layer over AZ91D magnesium alloy. 45 %, 40 % and 42 % improved corrosion resistance were observed in 72, 120 and 168 hours of exposure respectively in solution containing pH value of 7 and at molar ion concentration of 0.6 M.

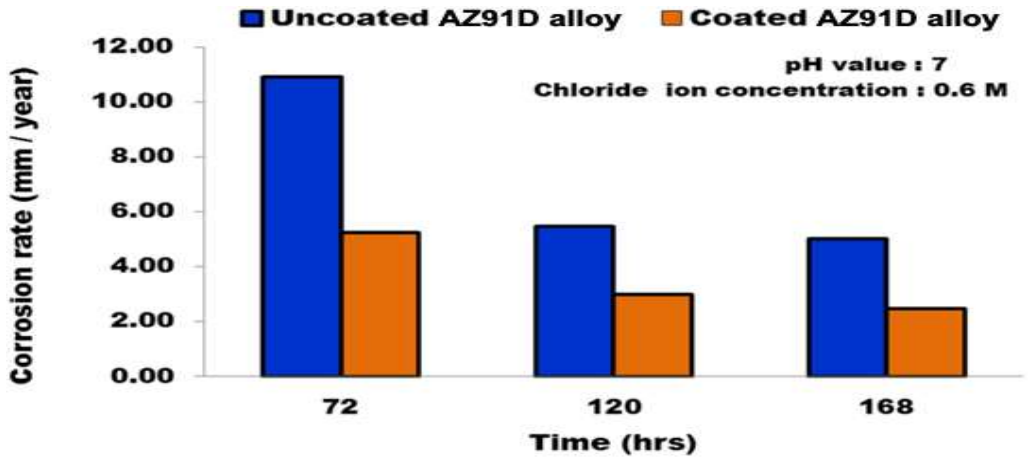

Fig. 16 Effect of time on corrosion rate

Figure 17 depicts the influence of exposure time on the corrosion rate of uncoated and coated AZ91D magnesium alloy. Uncoated and coated AZ91D magnesium alloy shows lack response in corrosion rate after one hour. This indicates that a diffusion barrier of corrosion product is likely to be MgO exists at the surface of the AZ91D magnesium alloy. When the exposure time is the increase rhe composition of diffusion barrier surface layer changes, as indicated by the differences in color of the product. AZ91D magnesium alloy appears to undergo dezincification. Dezincification can accrue by to mechanism, one mechanism involves the diffusion of zinc in to the surface of the alloy

where it undergoes preferential corrosion, leaving a copper rich residue. The other mechanism involves the corrosion of the AZ91D magnesium alloy and redepositing of magnesium as a porous layer. The average pit area is larger that indicates, few extremely large pits are available in the corroded region is shown in Fig. 17 (a). At lower exposure time, loss of carbide phase was observed due to severe localized deep corrosion attack. Visual examination of the samples after the test is revealed that the attack is in the form of localized etching around the carbide and metal interfaces in discrete regions of the sample. Further, it is noticed that the corrosion associated dense pitted areas show lot of cracks on the surface of corrosion film as shown in Fig. 17 (b). After 168 hrs of immersion, a little amount of corrosion pits were observed on the surface of the AZ91D magnesium alloy. The corrosion film on the specimen surface in the NaCl solution is considerably compacted, which is effectively prevents the further reaction takes place. Consequently, the growth rate of the film remains slow and forms shallower corrosion dimples (Fig.17 (c)) [44, 45]. In coated AZ91D magnesium alloy, a deep attack around the hard phase matrix interfaces over the entire surface and more severe attack in the coating matrix began to open up in some localized areas, leaving the carbide particles. Coated AZ91D magnesium alloy exhibits uniformly corroded surface, in which the carbide phase was clearly removed through loss of the supporting matrix as shown in Fig. 17 (d).As shown in Fig. 18 (a and b) the roughness measured by the atomic microscope on the corroded surface of the uncoated AZ91D magnesium alloy roughness value is not uniform and the surface was severely affected when increasing the exposure time. Similar trend was observed in the coated AZ91D magnesium alloy and the corroded surface is not uniform. Micro-holes left by carbide removal and localized discrete pits were found on the surface is the reason for the more undulations as seen in the AFM images (Fig. 18 (c and d).

Un coated AZ91D Magnesium alloy
pH value= 7 Corrosion time=36(h) Cl^- concentration = 0.6(M)

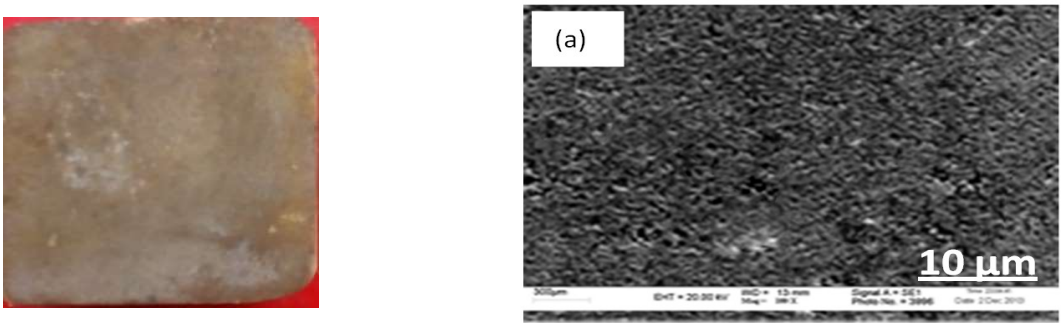

Coated AZ91D Magnesium alloy
pH value= 7 Corrosion time= 36(h) Cl^- concentration = 0.6(M)

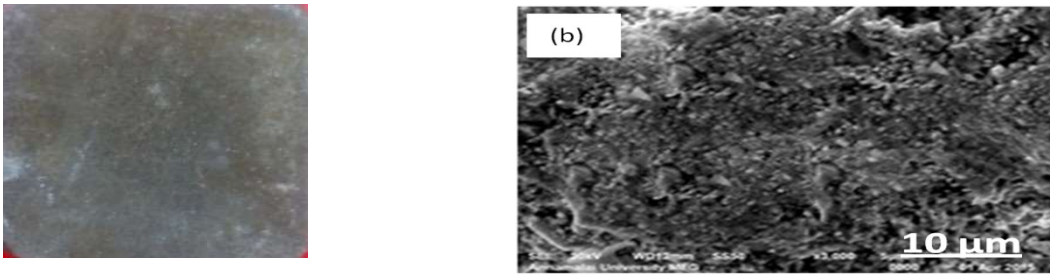

Un coated AZ91D Magnesium alloy
pH value= 7 Corrosion time= 168 (h) Cl^- concentration = 0.6(M)

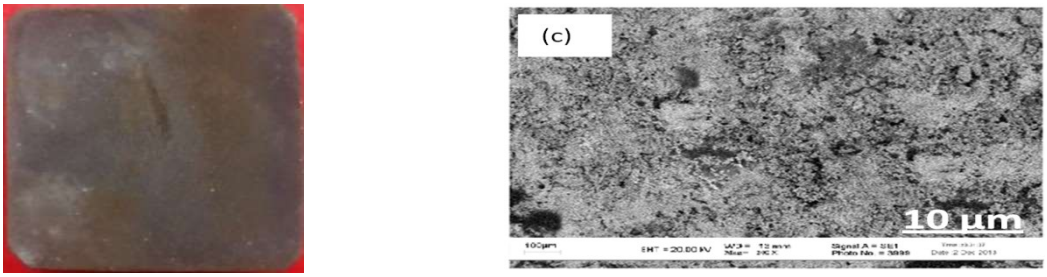

Coated AZ91D Magnesium alloy
pH value= 7 Corrosion time= 168 (h) Cl^- concentration = 0.6(M)

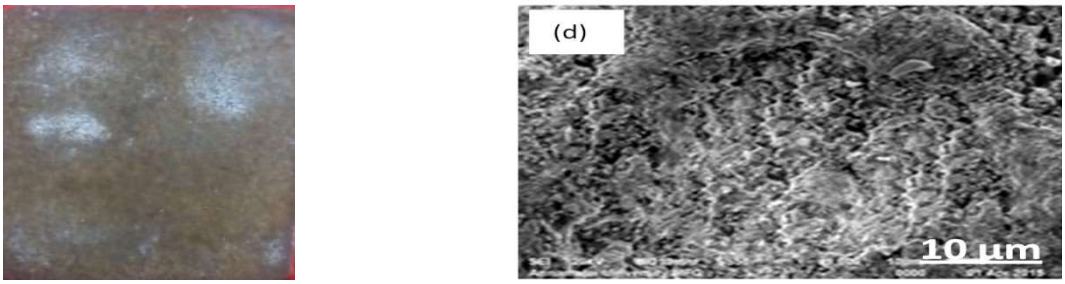

Fig. 17 Effect of time on corrosion morphology in immersion corrosion test specimens of uncoated and coated AZ91D Magnesium alloy

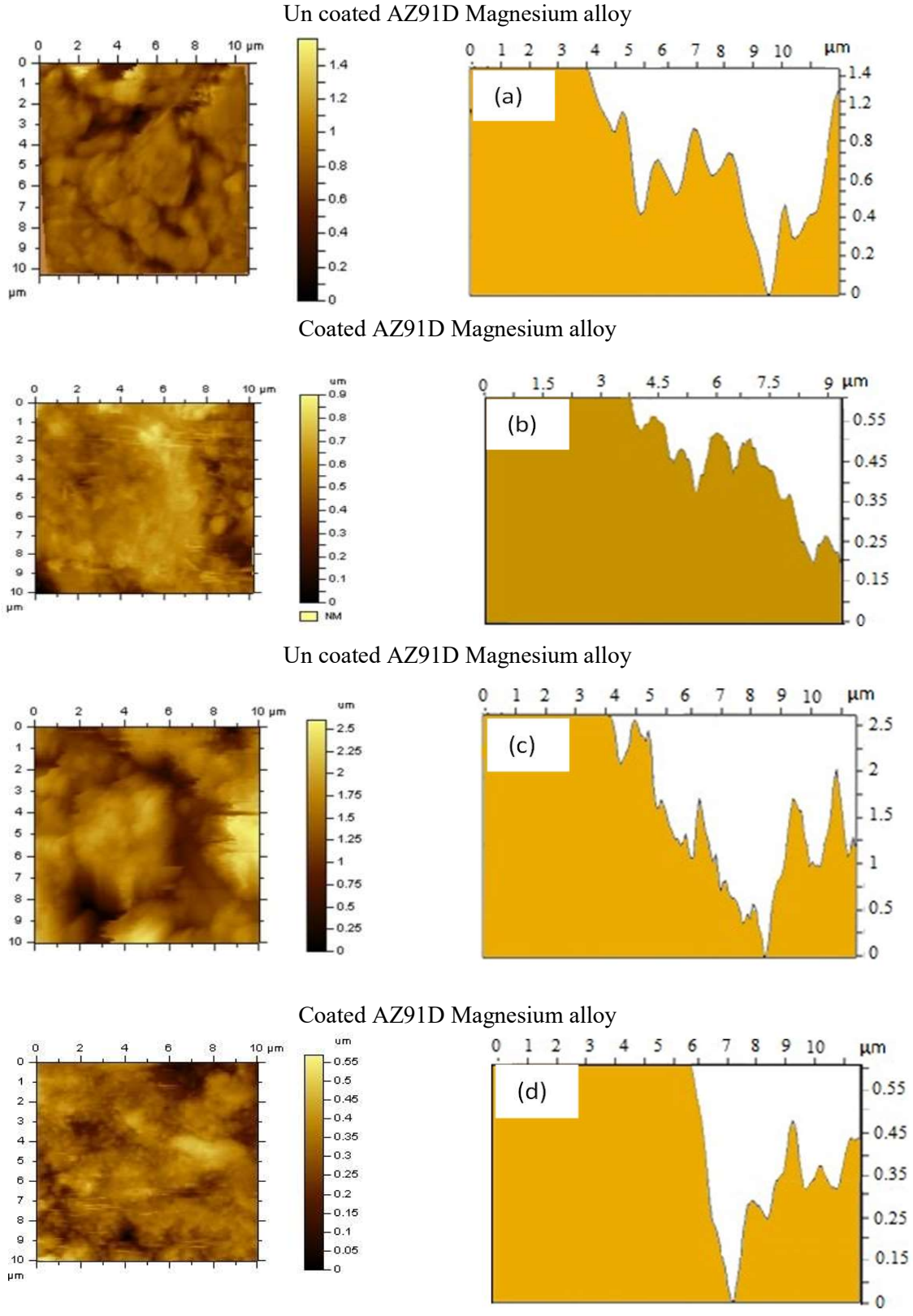

Fig. 18 Effect of time on corrosion morphology and pit depth of uncoated and coated Coated AZ91D Magnesium allo

4.0 Scanning Electron Microscopy Analysis

Figures 19 (a-d) show the SEM images of the corroded surfaces of uncoated and coated AZ91D magnesium alloy before and after the corrosion tests in 0.06 M NaCl solution for 9 hours in a neutral pH. It is observed from SEM images that the uncoated sample was affected by corrosion in 0.06 M NaCl. Before corrosion test, the surface of uncoated AZ91D magnesium alloy looks like a smooth surface without cracks or pits.The surface was corroded by NaCl solution as indicated by white big cavities are visible on the surface after corrosion tests (Fig. 19 a-b). The effect of NaCl is visible and it might be due to the breakdown of the chromium oxide layer by the attack of chloride ions released from NaCl solution. Breakdown of the chromium oxide layer allows progressively more chloride ions to penetrate through the barrier oxide layer that end up with allowing pitting corrosion. Hence, corrosion rate increases simultaneously. Figure 19 (c and d) show the SEM images of the corroded surfaces of coated AZ91D magnesium alloy before and after corrosion tests. It seems that the coatings protect the surface of AZ91D magnesium alloy from corrosion by NaCl to some extent. No visible effect of Cl^- ions can be noticed when comparing Fig. 19 (c and d). Hence, coated AZ91D magnesium alloy is effective in reducing the number of pits thus by reducing the corrosion rate. The anticorrosion effect of coating might be due to the uniform distribution of pores on the surface of coated AZ91D magnesium alloy. The formation of pores on the surface of coating was evolved as interconnected porosity which was developed during the coating process. Atomic force microscopic studies were carried out on the corroded specimens of uncoated and coated magnesium to evaluate the 3-D profile image, root mean square roughness (RMS) and average roughness (Ra).

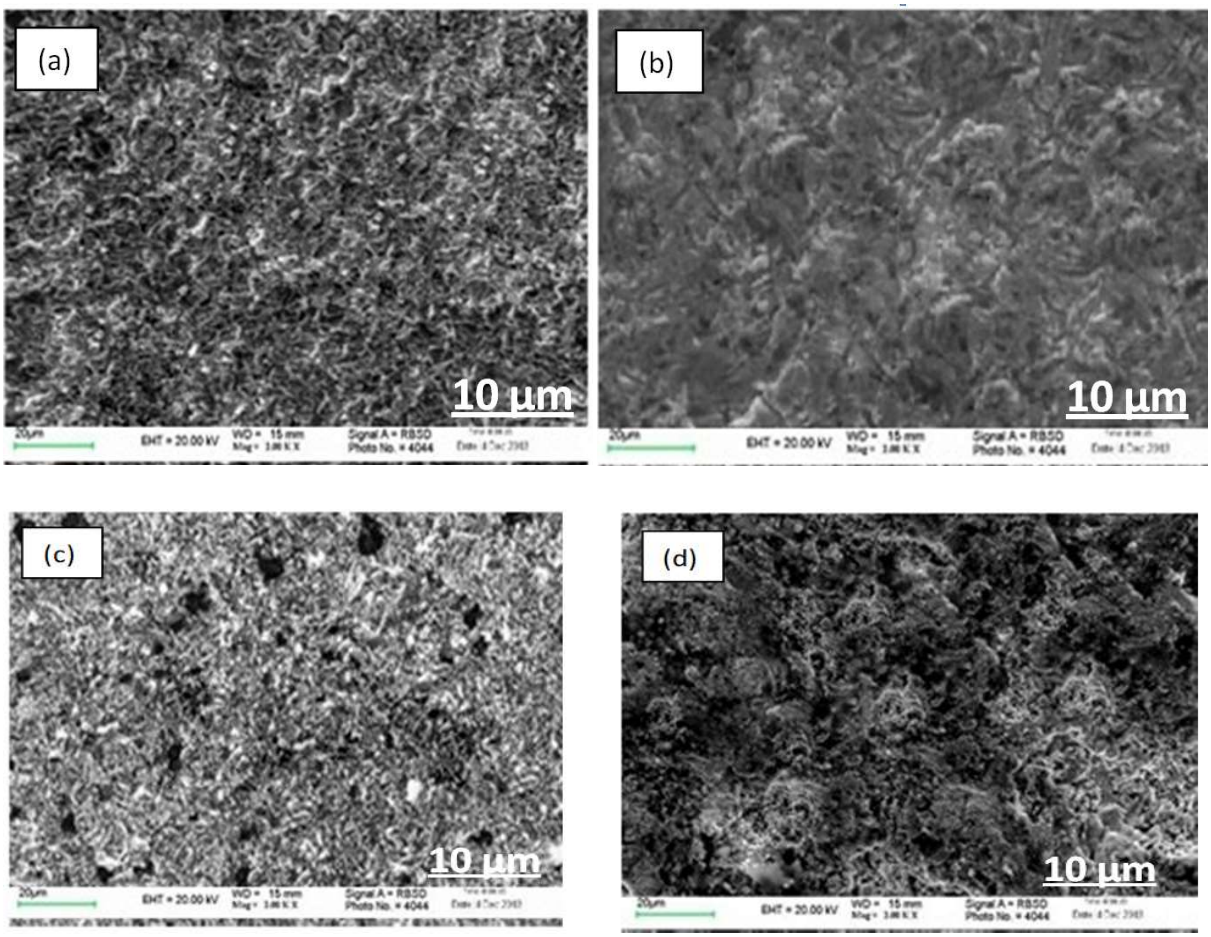

Fig. 19 SEM images of the corroded surfaces of uncoated and coated AZ91D magnesium alloy before and after the corrosion tests in 0.06 M NaCl solution for 9 hours in a neutral pH

AFM images show a marked difference in surface profile of uncoated and coated AZ91D magnesium alloy after the corrosion tests, the images of AZ91D magnesium alloy has the highest values of surface roughness and RMS, owing to the high rate of corrosion compared to coated AZ91D magnesium alloy (Fig. 20). Coated AZ91D magnesium alloy shows less undulation (Fig. 21). It suggests that the rate of corrosion in AZ91D magnesium alloy is higher than the coated AZ91D magnesium alloy in a corrosion

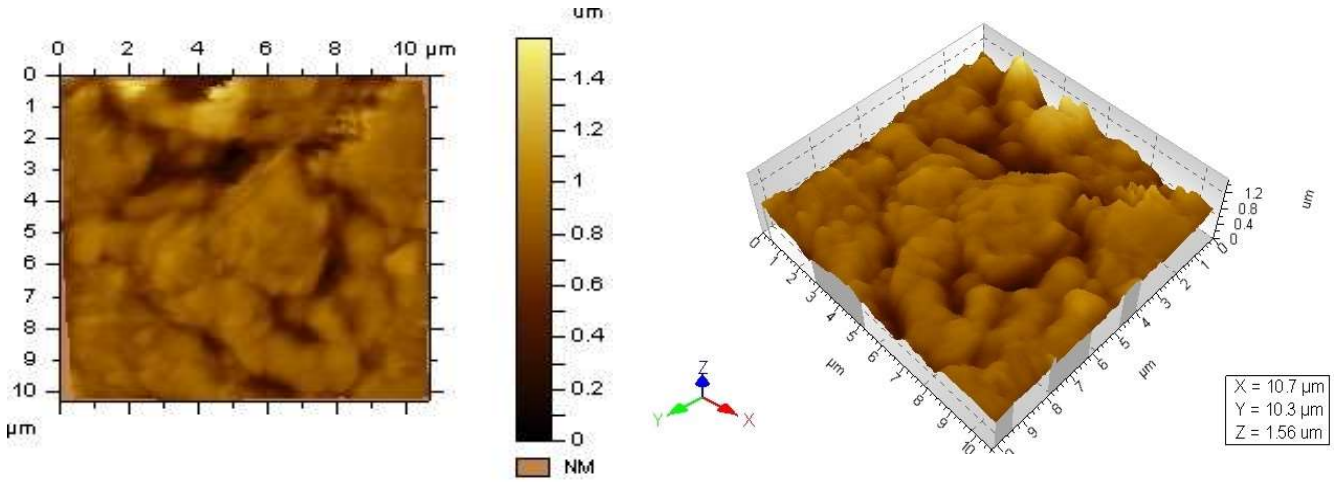

Fig. 20 AFM image of AZ91D alloy after immersion in 0.06 M NaCl for 9 hours

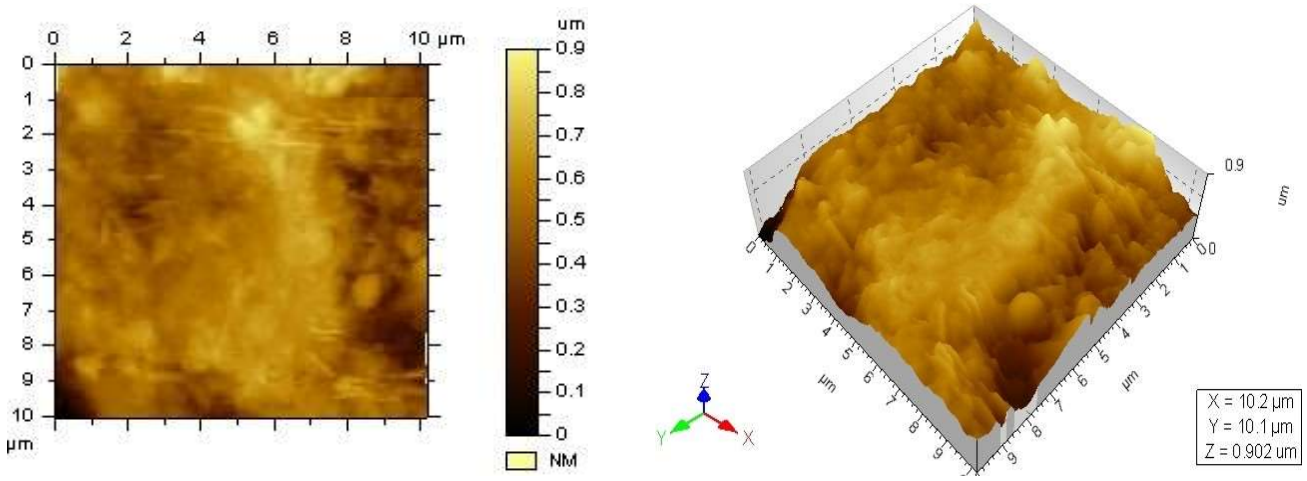

Fig. 21. AFM image of coated AZ91D alloy after immersion in 0.06 M NaCl for 9 hours

5. Conclusions

The following important conclusions are obtained from this investigation.

I. Empirical relationship was established to predict the corrosion rate of plasma sprayed stellite coatings on AZ91D magnesium alloy, incorporating chloride ion concentrations, pH value and immersion time. The developed relationship can be effectively used to predict the corrosion rate of stellite coatings on AZ91D magnesium alloy at 95% confidence level.

II. Design of experiment concept was effectively utilized to know the effect of corrosion parameters in immersion corrosion. Among the three parameters considered, pH level in the corrosion dominates the corrosion rate followed by Cl- concentration and exposure time.

III. In acidic NaCl solution (pH 3), the stellite coatings could not provide sufficient corrosion protection to magnesium alloy substrate in longer exposures. Stellite coatings were found to be highly susceptible to localized damage, and could not provide an effective corrosion protection to Mg alloy substrate in solutions containing higher chloride concentrations.

IV. Atomic microscope analysis shows that the corroded surface of uncoated AZ91D magnesium alloy shows higher Ra value is owing to the surface damage. Coated AZ91D magnesium alloy show less undulations on the analyzed region.

Acknowledgements

The corresponding author wishes to express his sincere thanks to the Annamalai University for extending facilities to characterize the coatings. The authors also wish to thank Mr. R. Selvendiran, Technical Assistant, CEMAJOR, Annamalai University for his help in carrying out this investigation.

REFERENCES

1. *Liuyan, Zhang Shuimei, Yang Xiao, Lv Xiaohua Jie, Wear and corrosion resistance of cold sprayed Cu-based composite coatings on magnesium substrate, J. Therm. Spray. Tech., Vol. 28, pp. 1212–1224, (2019).*

2. *T.S.Sidhu, S.Prakash, R.D.Agrawal, Hot corrosion studies of HVOF NiCrBSi and Stellite-6 coatings on a Ni-based superalloy in an actual industrial environment of a coal fired boiler, Surf. Coat. Technol., Vol.201, pp. 1602-161, (2006).*

3. *G.R.MirshekariDaee, S.Bonabi, S.F.Tavakoli, M.R.Shafyei, M .Safaei, Effect of interlayers on the microstructure and wear resistance of Stellite 6 coatings deposited on AISI 420 stainless steel by GTAW technique, Surf. Interface., Vol.9, pp. 79–92, (2017).*

4. *G.P.Rajeev, M.Kamaraj, S.R.Bakshi, Hardfacing of AISI H13 tool steel with Stellite 21 alloy using cold metal transfer welding process, Surf. Coat. Technol., Vol. 326, pp. 63-71, (2017).*

5. *S.Apay , B.Gulen , Wear properties of AISI 1015 steel coated with Stellite 6 by microlaser welding, Mater. & Des., Vol. 55, pp. 1-8, (2014.)*

6. *R.Singh, D.Kumar, S.K.Mishra., S.K.Tiwari, Laser cladding of Stellite 6 on stainless steel to enhance solid particle erosion and cavitation resistance, Surf. Coat. Technol., Vol. 251, pp. 87-97, (2014).*

7. *S.Houdkova, Z.Pala, E.Smazalova, M.Vostrak , Z.Cesanek , Microstructure and sliding wear properties of HVOF sprayed, laser remelted and laser clad Stellite 6 coatings, Surf. Coat. Technol., Vol. 318, pp. 129-41, (2017).*

8. *A.Frenk, W.Kurz , Microstructural effects on the sliding wear resistance of a cobalt-based alloy, Wear, Vol. 174, pp. 81-9, (1994).*

9. *A.Kusmoko, D.P.Dunne , H.Li , A Comparative study for wear resistant of Stellite 6 coatings on nickel alloy substrate produced by laser cladding, HVOF and plasma spraying techniques. Surf. Coat. Technol., Vol. 4, pp. 32-36, (2014).*

10. *F.Luo , R.Lupoi, A. Cockburn, M.Sparkes, W.ONeill , J-H.Yao , Characteristics of Stellite 6 Deposited by Supersonic Laser Deposition Under Optimized Parameters, J.Iron & Steel Res.Int., Vol. 20, pp. 52-7, (2013).*

11. *K.P. Rao, R. Damodaram , H.K.Rafi , G.D.J.Ram , G.M.Reddy , R.Nagalakshmi, Friction surfaced Stellite 6 coatings, Mater. Charact., Vol. 70, pp. 111-6, (2012).*

12. *F.W.Travis, W.Johnson , Explosive welding of Stellite to stainless steel, in: Tobias S.A.Koenigsberger F. (editors), Advances in Mach. Tool Des.& Res. Pergamon, pp.1319-32, (1968)*

13. *H.Yu , R.Ahmed , H.De, Villiers Lovelock , A comparison of the tribo-mechanical properties of a wear resistant cobalt-based alloy produced by different manufacturing processes, J.of.Tribol., Vol. 129, pp. 586-94,(2007).*

14. *H.Yu, R.Ahmed, H.D.V.Lovelock, S.Davies, Influence of manufacturing process and alloying element content on the tribomechanical properties of cobalt-based alloys, J.of.Tribol., Vol. 131, pp. 1-12, (2008).*

15. *A.Frenk, W.Kurz, Microstructural effects on the sliding wear resistance of a cobalt-based alloy, Wear, Vol. 174, pp. 81-91, (1994).*

16. *G.P.Rajeev ,M. Kamaraj, S.R.Bakshi , Hardfacing of AISI H13 tool steel with Stellite 21 alloy using cold metal transfer welding process, Surf. Coat. Technol., Vol. 326, pp. 63- 71, (2017).*

17. *R.Kaul , P.Ganesh , M.K.Tiwari, A.K.Singh, P.Tripathi, A.Gupta, A.K.Nath, Laser assisted deposition of graded overlay of Stellite 6 on austenitic stainless steel, Lasers in Engg.,Vol. 12, pp. 207-25, (2002).*

18. *G.P.Rajeev, M.Kamaraj, S.Bakshi, Hard facing of AISI H13 tool steel with Stellite 21 alloy using cold metal transfer welding process, Surf. Coat. Technol., Vol. 326, pp. 63-71, (2017).*

19. *B.Li , Y.Jin., J.Yao , Z.Li, Q.Zhang, Solid-state fabrication of WCp-reinforced Stellite-6 composite coatings with supersonic laser deposition, Surf. Coat. Technol., Vol. 321, pp. 386- 96, (2017).*

20. *G.P. Rajeev , M.Kamaraj , S.R.Bakshi , Hardfacing of AISI H13 tool steel with Stellite 21 alloy using cold metal transfer welding process, Surf. Coat. Technol., Vol. 326, pp. 63-71, (2017).*

21. *F.Findik, Recent developments in explosive welding, Mater.& Des., Vol. 32, pp. 1081-93, (2011).*

22. *AliArab,YansongGuo,QiangZhou,Pengwan Chen, Joining AlCoCrFeNi high entropy alloys and Al-6061 by explosive welding method, Vacuum., Vol. 174, pp. 109221, (2020).*

23. *K.P.Rao, R.Damodaram, H.K.Rafi, G.D.J.Ram, G.M.Reddy, R.Nagalakshmi, Friction surfaced Stellite6 coatings, Mater. Charact.,Vol. 70, pp. 111-6, (2012).*

24. *G.M.Reddy, K.S.Prasad, K.S .Rao, T.Mohandas, Friction surfacing of titanium alloy with aluminium metal matrix composite, Surf. Engg., Vol. 27, pp. 92-8, (2011).*

25. *N.Cinca, E.Lopez, S.Dosta, J.M.Guilemany, Study of Stellite-6 deposition by cold gas spraying, Surf. Coat. Technol., Vol. 232, pp. 891-8, (2013).*

26. *P.Richer, M.Yandouzi, L.Beauvais, B.Jodoin, Oxidation behaviour of CoNiCrAlY bond coats produced by plasma, HVOF and cold gas dynamic spraying, Surf. Coat. Technol., Vol. 204, pp. 3962-74, (2010).*

27. *T.S.Sidhu, S.Prakash , R.D.Agrawal , A comparative study of hot corrosion resistance of HVOF sprayed NiCrBSi and Stellite-6 coated Ni-based superalloy at 900°C, Mater.Sci. &Engg., Vol. 445-446, pp. 210-8, (2007).*

28. *T.S.Sidhu, S.Prakash, R.D.Agrawal, Studies of the metallurgical and mechanical properties of high velocity oxy-fuel sprayed Stellite-6 coatings on Ni- and Fe-based superalloys, Surf. Coat. Technol., Vol. 201, pp. 273-81, (2006).*

29. *B.S.Sidhu , S.Prakash , Studies on the behaviour of Stellite-6 as plasma sprayed and laser remelted coatings in molten salt environment at 900°C under cyclic conditions, J. of. Mater Proc. Technol., Vol. 172, pp. 52-63, (2006).*

30. *U.De Oliveira, V.Ocelik, and J. T. M. De Hosson, Microstresses and microstructure in thick cobalt-based laser deposited coatings, Surf. Coat. Technol., Vol.201, pp. 6363-6371,(2007).*

31. *D.Bartkowski, A.Bartkowska, Wear resistance in the soil of Stellite-6/WC coatings produced using laser cladding method. Int. J. Refract. Metals Hard Mater., Vol.64, pp. 20–26, (2017).*

32. *H.Y.Zhao, S.G.Liu, Y.S.Feng, J.P.Yao, Y.S.Xu, Failure analysis of desulfurization slurry circulating pump and HVOF coating protection technology progress, Appl. Mech. Mater. Vol.320, pp. 374–382, (2013).*

33. *C.R.Ciubotariu, D.Frunzaverde, G.Marginean, V.A.Şerban., A.V. Birdeanu., Optimization of the laser remelting process for HVOF-sprayed Stellite 6 wear resistant coatings, Optics & Laser Technol., Vol. 77, pp. 98-103, (2016).*

34. *D. Thirumalaikumarasamy, K. Shanmuga., V. Balasubramanian, Optimisation and sensitivity analysis of atmospheric plasma spraying parameters to minimise porosity in alumina coatings on AZ31B magnesium alloy, Int. J. Comput. Mater. Sci. Surf. Engg., Vol. 4, pp.1-24, (2013).*

35. *ASTM E3-95, Standard Practice for Preparation of Metallographic Specimens, ASTM International, West Conshohocken, PA, 2001*

36. *ASTM G31-72(2004), Standard Practice for Laboratory Immersion Corrosion Testing of Metals, ASTM International, West Conshohocken, PA, 2004,*

37. *K.Murugan, A.Ragupathy, V.Balasubramanian, K.Sridhar,Optimizing HVOF spray process parameters to attain minimum porosity and maximum hardness in WC–10Co–4Cr coatings, Surf. Coat. Technol., Vol. 247, pp. 90–102, (2014).*

38. *S. Garcia-Rodriguez, A.J. Lopez, B. Torres, J. Rams, 316L Stainless Steel Coatings on ZE41 Magnesium Alloy Using HVOF Thermal Spray for Corrosion Protection, Surf. Coat. Technol., Vol. 287, pp. 9-19, (2016).*

39. *R.Ambat , N.Aung, W.Zhou, Studies on the influence of chloride ion and pH on the corrosion and electrochemical behaviour of AZ91D magnesium alloy, J.Appl. Electrochem.,Vol. 30, pp. 865-874, (2000).*

40. *M.Carboneras, M.D.Lopez, P.Rodrigo, M.Campo, B.Torres, E.Otero, J.Rams, Corrosion behaviour of thermally sprayed Al and Al/SiCp composite coatings on ZE41 magnesium alloy in chloride medium, Corros. Sci., Vol. 52, pp. 761–768, (2010).*

41. *Mars Fontana, Corrosion Engineering, McGraw Hill Education; 3 edition, 2017*

42. *Lei Wang, Tadashi Shinohara, Bo-Ping Zhang, Influence of chloride, sulfate and bicarbonate anions on the corrosion behavior of AZ31 magnesium alloy, J. Alloys & Compd., Vol. 496, pp. 500–507,(2010).*

43. *J.Liang, P.Bala Srinivasan, C.Blawert, W.Dietzel. Influence of chloride ion concentration on the electrochemical corrosion behaviour of plasma electrolytic oxidation coated AM50 magnesium alloy, Electrochim. Acta., Vol. 55, pp. 6802–6811, (2010).*

44. *M. Carboneras, M. D. Lopez, P. Rodrigo, M. Campo, B. Torres, E. Otero and J. Rams. Corrosion behaviour of thermally sprayed Al and Al/SiCp composite coatings on ZE41 magnesium alloy in chloride medium, Corros. Sci., Vol. 52, pp. 761–768, (2010).*

45. *Campo M, Carboneras M, Lopez M D, Torres B, Rodrigo P, Otero E and Rams J Corrosion resistance of thermally sprayed Al and Al/SiC coatings on Mg, Surf. Coat. Technol., Vol. 203, pp. 3224–323, (2009).*